



**Ball Aerospace
& Technologies Corp.**



JPL Document D-68673 Rev A

TECHNOLOGY DEVELOPMENT FOR EXOPLANET MISSIONS

Technology Milestone Whitepaper

Advanced Speckle Sensing for Internal Coronagraphs

Stephen E. Kendrick, PI

Ball Aerospace & Technologies Corp., Boulder CO

Stuart Shaklan (Co-I), Jet Propulsion Laboratory

Charley Noecker, (Co-I), Jet Propulsion Laboratory

Jeremy Kasdin, (Co-I), Princeton University

Ruslan Belikov (Co-I), NASA Ames Research Center

Original version 29 April 2011

Revised 28 November 2011

National Aeronautics and Space Administration
Jet Propulsion Laboratory
California Institute of Technology
Pasadena, California

© 2012. All rights reserved.

APPROVALS

Released by

 2/6/12

Stephen E. Kendrick

Ball Aerospace & Technologies Corp.

Approved by

 2/6/12

Peter R. Lawson

Exoplanet Exploration Program Chief Technologist, JPL

 2/6/12

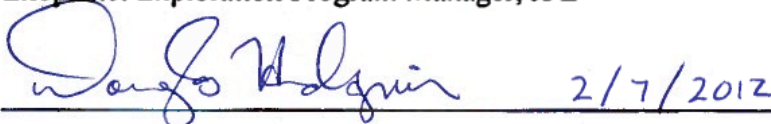
Marie Levine

Exoplanet Exploration Program Technology Manager, JPL

 2/6/2012

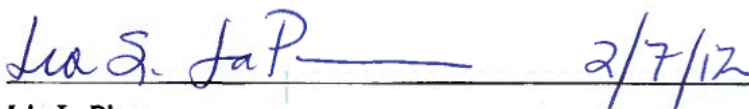
Michael Devirian

Exoplanet Exploration Program Manager, JPL

 2/7/2012

Douglas Hudgins

Exoplanet Exploration Program Scientist, NASA HQ

 2/7/12

Lia LaPiana

Exoplanet Exploration Program Executive, NASA HQ

Summary

Advanced Speckle Sensing for Internal Coronagraphs (ASSIC) is a study of two advanced methods for measuring residual wavefront errors in spaceborne internal coronagraphs. The coronagraph instrument suppresses starlight by a factor of about 10 billion, so that the starlight “speckles” from residual wavefront errors are as faint as the exoplanets we hope to see. These speckles are a significant threat to detection of Earth-sized exoplanets, particularly if they change with time. With the traditional speckle-nulling measurement technique,¹³ measuring these very faint speckles, to monitor and correct them, takes roughly as long as detecting the faint exoplanets; in the presence of zodiacal and exozodiacal dust backgrounds, it takes typically many hours or days. The prevailing strategy for managing these speckles has been to impose stringent thermal and mechanical stability requirements on the entire optical system, so that the speckles remain stable long enough to measure and correct them and then conduct a planet-search observation. The proposed advanced sensing methods are expected to improve the speed of speckle measurements, allowing frequent and accurate adjustments of the instrument to reduce them. This speed improvement, if validated, would completely change the technology landscape for such missions. It would dramatically reduce the timescale for stability requirements on the telescope and instrument optical train. These methods appear to be applicable to all the leading candidates for internal coronagraph instrument: band-limited Lyot, shaped pupil, pupil remapping, and perhaps vortex and visible nulling coronagraphs.

Table of Contents

1. Objective	1
2. Introduction	1
2.1. Milestone: Demonstration of coherent speckle detection in an internal coronagraph	2
2.2. Speckle Detection Methods	5
2.3. Differences between flight and laboratory	9
3. Milestone Procedure	9
3.1. Definitions	10
3.2. Measurement of the Star Brightness	13
3.3. Measurement of the Coronagraph Contrast map	14
3.4. CSD Measurement of the Coronagraph Speckle Field	14
3.5. Milestone Validation Procedure	15
4. Success Criteria	16
4.1. Light source	16
4.2. Contrast performance	16
4.3. Incoherent stray light background	16
4.4. Duration and robustness	17
5. Certification Process	17
5.1. Milestone Certification Data Package	17
6. References	18
Appendix A. Uncertainty and integration time analysis	21

1. Objective

In support of NASA’s Exoplanet Exploration Program and the ROSES Technology Development for Exoplanet Missions (TDEM), this whitepaper explains the purpose of the TDEM Milestone for Advanced Speckle Sensing for Internal Coronagraphs, specifies the methodology for computing the milestone metric, and establishes the success criteria against which the milestone will be evaluated.

2. Introduction

This Technology Milestone serves to gauge the developmental progress of technology for a space-based coronagraph mission, such as ACCESS, that would detect and characterize exoplanets, and the mission’s readiness to proceed from pre-Phase A to Phase A. Completion of this milestone is to be documented in a report by the Principal Investigator and reviewed by NASA HQ. This milestone addresses calibration of starlight suppression. The approach for accomplishing the milestone is similar to the one implemented for TPF-C Milestone #1 and TPF-C Milestone #2, which demonstrated narrow band (#1) and broadband (#2) starlight suppression on the High Contrast Imaging Testbed (HCIT). The main differences for this milestone reside in the use of a starlight reference beam and the emphasis on accurate measurement of stellar speckles rather than solely their suppression.

An internal-occulter coronagraph on an unobscured telescope¹ forms an image of the star and planet, and then blocks the star with a small spot, called a coronagraph field occulter (CFO). The planet light goes past the CFO and reaches the detector with little attenuation. A 4 m diameter telescope is considered appropriate for a capable mission to detect Earth-sized planets in the habitable zones (HZs) of nearby stars; telescopes as small as 1.5 m have been proposed for observing Jupiter-like exoplanets.^{2,3,4}

Ordinary Fraunhofer diffraction of the aperture allows substantial leakage of the starlight around the CFO (commonly 10^{-4}) even with a perfect telescope (Figure 1). To combat this, several elaborate methods have been devised to allow very low transmission of the star (10^{-10}) while allowing high transmission for the planet at a small angular separation. The inner working angle (IWA) is the smallest practical angle for planet detection at a given planet-star contrast, as limited both by static characteristics of the design and by wavefront control and other challenges. For these instruments, it is convenient to express angular separations and the IWA in units of λ/D , where λ is the observing wavelength and D is the telescope diameter. The angle λ/D is also approximately the full-width at half-maximum (FWHM) of the telescope’s point spread function. The most aggressive designs appear capable of an IWA of $2 \lambda/D$; more conservative designs have an IWA of 3-5 λ/D . It is still uncertain which of these are practical for a space mission, because they have very different wavefront control requirements.

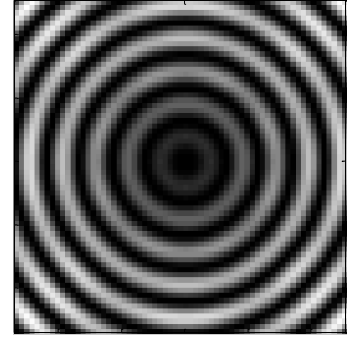


Figure 1. Immediately after the CFO, before the Lyot stop. Airy rings persist in the image, with brightness $\sim 10^{-4}$ of peak.

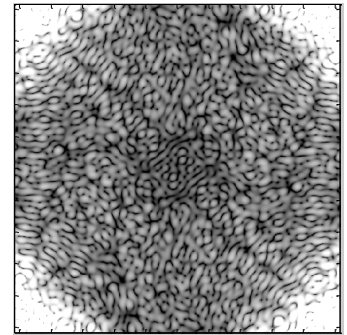


Figure 2. Model of residual starlight speckles on final focal plane after wavefront is tuned by a DM. Average stellar leakage $\sim 10^{-10}$ of peak. Zodi signals are not shown.

Technology Milestone Whitepaper
Advanced Speckle Sensing for Internal Coronagraphs – Kendrick

After the star's point spread function (PSF) is suppressed, small wavefront errors in the telescope and instrument will lead to leakage of starlight in the form *speckles* of starlight on the detector (Figure 2), which will increase the required integration times and create systematic error signals mimicking a planet. A deformable mirror (DM) can correct the wavefront errors that cause those speckles, over some limited range of wavelengths ($\Delta\lambda/\lambda$ potentially up to 20-25%). By carefully measuring the speckle intensities and adjusting the DM, we can reduce them to the brightness of the planet. Typical final adjustments of the DM are a small fraction of an angstrom (\AA), 10^{-10} m. At the end we may have thousands of speckles, all roughly the same size and brightness as the planet. Isolating the real planet from these speckles is the big challenge.

If the speckles were absolutely stable, their only impact would be a modest amount of shot noise. Then we could allow them to be as bright as the local and exozodi, because a little longer integration time would fully compensate. But the speckles can have systematic fluctuations, which don't average down nicely with integration time; in fact, the resulting uncertainty can constitute a sensitivity floor for arbitrarily long integrations. We must choose an average speckle brightness faint enough that the systematic fluctuations can be managed to fit within the signal-to-noise ratio (SNR) budget. Consequently the speckles are faint and hard to measure.

That means direct speckle intensity (DSI) measurement is time-consuming and difficult. Typically, the speckle brightness must be calibrated with an uncertainty less than 10-15% of the faintest planet signal we hope to see, and it must be stable over the time needed to calibrate the speckles and take one planet measurement. For a mag 1 star, a 20% passband, and a 1.5 m diameter telescope with a basic Lyot coronagraph, it takes a day to measure mag 26 speckles to an SNR of 10, consistent with detection of Earth-size exoplanets. And 10% stability of that speckle requires wavefront stability of order 0.1 \AA or better. It is very difficult to maintain passive wavefront stability below an angstrom for a day or more on orbit, and testing the flight hardware in the lab to verify that requirement is well beyond the current state of the art.

2.1. Milestone: Demonstration of coherent speckle detection in an internal coronagraph

The central purpose of this laboratory demonstration is to demonstrate methods of measuring and perhaps controlling the residual starlight (speckles) on the science focal plane of an internal coronagraph via coherent speckle detection (CSD). We will show these methods are capable of sensing speckles with the required accuracy and with the predicted improvement in speed. These methods entail crafting a reference beam from the core of the stellar image, and using coherent methods such as Mach-Zehnder interferometry to identify, isolate, and measure the speckle fields. As shown below, we expect that adequate SNR can be achieved in a shorter time than with DSI measurements, and this is the primary reason for trying this approach. The requirement for this milestone is:

Using coherent speckle detection methods, demonstrate the capability to measure speckles of 1×10^{-8} contrast with uncertainty, stability, and repeatability of 20% in intensity and 1 radian in phase with 90% statistical confidence, in a window at least $2 \times 2 \lambda_0/D$ wide at $< 10 \lambda_0/D$ from the star, in one spectral band of width $> 10\%$, with a uniform incoherent background of at least 1×10^{-8} in the area covered by the PSF.

CSD methods are described below. Contrast is defined as the brightness per pixel on the speckle as a fraction of the brightness per pixel on the peak of the unblocked stellar image. The inner

Technology Milestone Whitepaper
Advanced Speckle Sensing for Internal Coronagraphs – Kendrick

working angle (IWA) is the minimum angular radius from the central core of the stellar image at which the residual starlight is fainter than some threshold, in our case 1×10^{-8} of the peak; typically this threshold is equal to the goal for sensitivity to exoplanets. Speckle amplitude and phase refer to the amplitude and phase of the optical field that causes the observed speckle intensity. Radial angles from the star are commonly scaled to the characteristic size of the PSF on the sky, λ_0/D , where λ_0 is the central wavelength of the passband and D is the telescope diameter. In the laboratory, without a telescope, we refer to the equivalent distance in the focal plane, $f\lambda_0/D = \lambda_0 F$, where f and $F=f/D$ are the equivalent focal length and f-number of a telescope producing the same beam at the coronagraph entrance. We adopt a relaxed requirement for the IWA because this study emphasizes measuring and controlling the speckle brightness, not minimizing the IWA. The milestone measurement may be satisfied anywhere in the normal suppression region of the instrument, i.e. between the inner and outer working angles. The incoherent background is from any light source which cannot produce detectable interference with the “star” source.

The milestone relates to progress demonstrated in the JPL High Contrast Imaging Testbed (HCIT), using the Lyot coronagraph table. The chosen mean speckle intensity (10^{-8}) is sufficiently routine on HCIT that it will not consume an inordinate amount of time to establish the initial conditions of the experiment. The speckle intensity verification accuracy goal is only a factor 10 greater than the requirement for detection of Jupiter-like exoplanets. And the brightness of incoherent background (10^{-8}) is comparable to that of a Solar-System-twin exozodi cloud. The phase requirements are consistent with the use of these advanced speckle detection methods for closed-loop wavefront control. We will conduct experiments to attempt closed-loop operation with CSD measurements, but it is not a requirement for the Technology Milestone.

Demonstration of milestone performance must be stable and repeatable, thereby demonstrating that the result is not spurious or transient. We will repeat the milestone demonstrations in order to build up statistical significance at the 90% confidence level, as further described in Section 3.1.11.

We will develop optical models and uncertainty budgets for this experiment. We will seek consistency of these models with the demonstrated results, to establish that the behavior is thoroughly understood. An uncertainty model for coherent speckle detection performance has also been developed by the study team (Appendix A). Unless there are significant unanticipated systematics in the measurement, we expect to validate this model commensurate with the improvement in test data. A detailed physics-based model of optical wave propagation in the coronagraph and the response to CSD reference beams is straightforward to assemble from existing code. We may encounter systematics of yet-unknown origin, and if so, we will try to characterize and eventually identify and control them, with the aid of more detailed optical models. If this is successful, a preliminary uncertainty budget at the milestone contrast level based on these models will be included with this milestone report, although there are no milestones applying to either optical models or uncertainty budgets.

In addition we will work toward an unofficial progress goal as follows:

Using coherent speckle detection methods, demonstrate the capability to measure speckles of $\sim 1 \times 10^{-7}$ contrast with uncertainty, stability, and repeatability of 20% in intensity and 1 radian in phase at $< 10\lambda_0/D$ inner working angle in one spectral band of width $> 10\%$ with a uniform incoherent background of at least 10^{-7} in the area covered by the PSF.

Technology Milestone Whitepaper
Advanced Speckle Sensing for Internal Coronagraphs – Kendrick

This goal relates to progress demonstrated in the first year at the Princeton coronagraph testbed, which operates in air. This effort is meant as intensive practice for the Milestone effort; the key products are procedures, algorithms, and lessons-learned that will smooth the way in HCIT. The chosen speckle intensity goal is modestly easier than the performance that has been shown already there, but the goal for verification accurate to 20% represents a significant tightening of knowledge requirements. The speckle phase is the optical phase of the field that causes it.* Meeting this goal will require mastery of speckle measurement techniques, at a level commensurate with the challenge of working in air.

Table 1 shows a possible sequence of steps to increase the maturity of CSD techniques in HCIT. The present study is the first in that sequence. “Sensing accuracy” means the accuracy of CSD speckle measurements in intensity and phase. “Mean speckle brightness” is the level of residual speckles, scaled to the peak of the unblocked stellar PSF, at the beginning of CSD measurements. “Max incoherent brightness” is the highest surface brightness of non-interfering light on the science detector, scaled to the peak of the unblocked stellar PSF. (This light may be turned off at times.) “Individual passband” is the full width $\Delta\lambda/\lambda$ for a single experiment; “multiple passbands” is a wider wavelength range which can be covered by a sequence of such experiments over a few hours. “Speckle subtraction or CDI” (coherent difference imaging) is the accuracy with which residual speckles can be subtracted after active control loops have run to a state

Table 1 A vision for a sequence of milestones to bring each CSD technique to maturity for flight. Shading indicates a change from the previous milestone.

	MS1	MS2	MS3	MS4	MS5
Sensing accuracy	20%, 1 rad	20%, 1 rad	10%, 0.5 rad	10%, 0.5 rad	10%, 0.5 rad
Mean speckle brightness	10^{-8}	2×10^{-9}	10^{-9}	10^{-9}	10^{-10}
Max incoherent brightness	10^{-8}	10^{-8}	10^{-7}	10^{-7}	10^{-7}
Individual passband	10%	20%	20%	20%	20%
Controlled FOV	Square, $2 \times 2\lambda/D$	D-shape, $4-10\lambda/D$	D-shape, $3-10\lambda/D$	D-shape, $3-10\lambda/D$	D-shape, $3-10\lambda/D$
Active speckle control		Yes	Yes	Yes	Yes
Speckle subtraction (CDI)				15%	15%
Multiple passbands				400-900nm	400-900nm
OTA simulator (WFE)				Yes	Yes

of completion. (This requires that CSD sensing accuracy is not the principal limitation for the achieved mean speckle brightness.) And an “optical telescope assembly (OTA) simulator” would be used to impose wavefront error (WFE) in amplitude and phase onto the incoming light, to simulate the static and dynamic errors in the telescope within some assigned tolerances.

It may be useful to spread this work into a larger number of milestones. The capability after MS4 is sufficient for an instrument for direct detection and spectroscopy of Jovian exoplanets with a

* Optical phase will vary much less than 1 radian in a 20% passband, unless the optical field is near a zero-crossing, which would imply the intensity there is especially faint.

1.5-2 m telescope. The capability after MS5 is sufficient for direct detection and spectroscopy of Earth-twin exoplanets with a 4m telescope.

The definitions of technology readiness levels (TRLs)⁵ are not explicit about the role of performance requirements in rating TRLs below 5. Indeed, a key question for technologies like our coronagraphs is whether technology readiness for a given flight performance requirement is credibly proven by an experiment showing a poorer performance level; typically it is not seen as credible, because of “unknown unknowns” that could be limiting the experimental result. But after HCIT performance with CSD* (*i.e.*, using breadboard hardware with laboratory software and computers) meets the requirements of a particular flight mission, such as a Jovian exoplanet direct detection mission, then we can assert that it has reached TRL 4 for that target performance. That occurs at MS4 in Table 1; similarly MS5 would establish TRL 4 for an Earth-like exoplanet direct detection mission. Progress to TRL 5 would occur as the HCIT with CSD is improved to a brassboard level, and so on.

2.2. Speckle Detection Methods

There are several existing methods for isolating speckles from planets:

- ❖ **Direct Speckle Intensity (DSI) measurements** use intensities from ordinary images.
 - **Angular Difference Imaging (ADI)**, also known as roll deconvolution,^{6,7,8} compares images—intensity patterns—in which the speckles remain stable on the detector while the planet moves. Two or more images are taken at different telescope roll angles around the line of sight. The difference between the images tends to subtract speckles, which rotate with the telescope, from astrophysical sources, which stay fixed on the sky and thus move on the focal plane image. This is the measurement and control concept for the most recent version of the TPF-C mission concept⁹ and most of its smaller cousins.
 - **Spectral Difference Imaging (SDI)**^{10,11,12} makes use of the different spectral behavior of speckles and planets. The speckle’s position in the focal plane moves radially outward almost linearly with increasing wavelength, while the planet’s position is invariant. Measuring a focal plane image in each of several passbands can be compared to form a model of the star spectrum and the wavefront that caused the speckles in each image.
 - **Speckle nulling.**¹³ Mainly viewed as a procedure for minimizing the brightness of speckles in the focal plane, speckle nulling (SN) incorporates a technique for estimating the amplitude and phase of the speckle field. The speckle brightness is a measure of its field amplitude; to null that speckle, we try to generate the same field amplitude at that image plane location but opposite phase. We do that by imposing a cosine wave on the DM (typically sub-nm amplitude) that diffracts starlight there; we know the necessary amplitude but initially not the phase. So we try that cosine wave with a series of phase offsets, and determine the best-fit phase from the speckle brightnesses in those trials. Finally, we may minimize that speckle’s brightness by imposing a cosine onto the DM with this fitted phase. However, if we omit this final step, the speckle will not be minimized, but its amplitude and phase will be known. To date SN has only been applied in narrow band light. Thus it is not suitable for use in our broad-band milestone.

* We have concluded that it is not sensible to assign a TRL to CSD itself, but only to HCIT using CSD methods.

- ❖ **Coherent Speckle Detection (CSD)** measurements use images of interference between speckles and a brighter stellar reference beam, exploiting their mutual coherence. Companion algorithms yield estimates of the speckle fields and/or needed DM corrections.
 - **Phase Diversity (PD).**^{14,15,16,17} A reference field is created at the science detector by means of a “phase diversity” perturbation introduced at the DM. Images are taken of the interference between the speckles and the reference beam. We must choose a suitable PD perturbation to impose on the DM, that spreads the field widely enough in angle to pass through the coronagraph stops and reach the detector with a sufficiently uniform and predictable profile. A grid of lines or spikes on the DM actuators seems appropriate.¹⁵ We may also wish to vary the PD perturbations to exercise the reference beam phase; this can be done by shifting the lines or spikes across the DM.*
 - **Mach-Zehnder interference using a pinhole (PH).**^{18,19,20,21} A reference beam is crafted from the central core of the stellar image and carried via a separate path to meet the speckle fields at a detector. Images are taken of the interference between the speckles and the reference beam. In some configurations it is possible to vary the reference beam phase to gather quadrature phase information. In this experiment we will employ a set of pinholes arranged to the side of the Lyot stop. These pinholes will be exposed in turn to act as reference beams. We refer to this as PH-CSD or simply PH.

We will compare PD to PH to determine the accuracy of speckle intensity and phase measurements.

The speckles are created by small errors in the telescope, and they are *coherent* with the starlight, i.e. they can have interference fringes that are mutually reinforcing across a wide spectral band. The exoplanet and exozodi light are incoherent with the star, i.e. they have a random phase relationship, and thus show no interference effects.

All of the CSD methods use a known wavefront disturbance or other means of generating a starlight reference beam, which is brought into interference with the residual speckle fields for either detection or correction. The interference term (see Equ. A.1, page 21) distinguishes stellar speckles from the incoherent zodi and planet signals, and with a sufficiently strong reference beam, it also offers “heterodyne amplification,” i.e. the heterodyne cross-term can be larger than the speckle intensity alone. That in turn allows quicker speckle measurements against a zodi background. The CSD results can be used for closed loop control of the DMs to suppress the speckles, but primarily they have been used to demonstrate post-processing of the data to subtract the CSD-derived estimate of speckle flux.^{15,17} In this study we aim to improve our understanding of the CSD-derived speckle information, and show the limits of those techniques. CSD speckle measurements lead to estimates of equivalent speckle intensity, which can be compared to DSI measurements of the same speckles.

As we will show, CSD can accommodate an exozodi much brighter than our own. In fact, the calibration integration time is nearly constant with increasing exozodi brightness, as long as the reference beam brightness rises with it. Thus we can keep the calibration-observation cycle short, so instrumental drift is no worse for a high-exozodi star than a low-exozodi star. Thus the limit-

* We are not discussing here the technical difficulties with the DM that complicate this procedure; but the excellent results in HCIT¹⁶ indicate that these technical problems are mild enough to allow some success with PD-CSD.

Technology Milestone Whitepaper
Advanced Speckle Sensing for Internal Coronagraphs – Kendrick

ing delta-magnitude in exoplanet sensitivity, expected to arise from systematic drift (Section 2.2 of Ref 1), will be constant vs. exozodi. By contrast, for traditional direct speckle measurements, increasing exozodi lengthens the timescale for calibration proportionally, practically ensuring a degradation of limiting delta-magnitude (planet sensitivity).

The study will demonstrate a robust capability to measure the speckles by CSD and correct or subtract them, and will verify the accuracy of the measurements over a full passband. Speeding that measurement has the following benefits:

- (a) speeding the exoplanet observation cycle and improving the observing efficiency;
- (b) relaxing the stability requirements on the telescope and following optics;
- (c) operating with more aggressive inner working angle (IWA);
- (d) devising verification methods that are closer to the current state of the art; and
- (e) improving robustness to high exozodi levels.

We plan to test the PD and PH techniques on HCIT, and to compare the speckle fields to each other. We will design modifications to the existing Princeton and HCIT testbeds to enable experiments with the new techniques. We will develop test procedures and algorithms for analyzing focal plane data—principally fitting a speckle field plus a spherical wave to the observed intensity profiles. We will implement the necessary hardware modifications, conduct the testing, and analyze the data to estimate the CSD-derived speckle intensity and direct speckle measurement, and thus demonstrate sensing performance. Wavefront errors will be corrected during these measurements mainly to ensure the quality of the data; but the early focus will be on CDI post-processing to subtract the measured speckles rather than speckle suppression. If resources allow, we will turn attention to using the speckle measurements in a closed loop control system.

In addition, we will develop physics-based performance models of the experiment, including the initial wavefront, the DM’s response to commands, propagation of waves through the system, drift and jitter in alignment, interference at the detector array, and detection noise, for both methods of coherent detection. We will attempt to validate these models by comparison with measured data. In future studies we will use the validated models to develop predictions of on-orbit performance, and compare the predictions with typical flight requirements, to provide benchmarks for future experiments.

2.2.1. Previous experimental work

Previous work on calibrating and suppressing or subtracting speckles has laid a firm foundation for this study, but each falls short in some way of the needs of a probe-class mission.

Trauger and Traub²² simulated an ADI measurement (angular differencing) using an actual time sequence of HCIT measurements with a band-limited Lyot coronagraph. This achieved sensitivity below that needed for a probe-class mission to find Jupiter-like planets, but was a narrowband demonstration ($\Delta\lambda/\lambda=0$) and used direct speckle detection.

Belikov and the Princeton group²³ demonstrated the SDI technique (spectral differencing) using speckle position changes with wavelength to discriminate them from the planet. They achieved $\sim 10\times$ improvement in speckle suppression at low contrast (from $\sim 10^{-5}$ to $\sim 10^{-6}$), but the planet also was partially suppressed, and this effect got worse at smaller angles from the star. Biller *et al.*²⁴ did an SDI experiment at HCIT with the band-limited Lyot coronagraph at much higher contrast. Those measurements used 5 adjacent filters with $\Delta\lambda/\lambda=2\%$, and found substantial differences in the speckles from different passbands. This is a warning for our CSD studies, that we

Technology Milestone Whitepaper
Advanced Speckle Sensing for Internal Coronagraphs – Kendrick

may find rapid spectral variations. As we said before, SDI measurements are based on direct speckle detection, and accordingly suffer from the same weaknesses vs. CSD.

The Princeton group have also demonstrated CDI^{15,25}—subtracting the CSD estimate from the raw image, leaving the incoherent signal from planets and zodi. This was done with shaped pupils and laser light. Later experiments by the same group at HCIT¹⁷ took advantage of its improved contrast, and added the matched filtering concept, which gave a factor ~ 1.7 improvement in uncertainty in the subtracted CSD contribution. Guyon *et. al.*²⁶ have also applied CDI at the Subaru testbed, and developed statistical techniques to validate the CSD estimates.

Table 2 Performance results for several experiments on isolating planets from speckles.

	Trauger ²²	Belikov ²³	Biller ²⁴	Give'on ¹⁵ Belikov ²⁵	Belikov ¹⁷	Guyon ²⁶
Technique	ADI	SDI	SDI	CDI	CDI	CDI
Optical bandwidth	0	0 (2 lasers)	2%	0	2%	0
Angular range	4-10 λ /D	5-14 λ /D	5-14 λ /D	5-14 λ /D	4-10 λ /D	1.65-4.4 λ /D
Raw contrast:	6e-10	1e-5	1e-6 to 1e-9	6e-7	1.2e-9	2.3e-7
Incoherent light estimate	–	–	–	6e-7	8.8e-10 $\pm 1.5e-10$	1.6e-7
Coherent light estimate	–	–	–	9e-8	6.5e-10	3e-9 $\pm 4.5e-8$
Stability (rms, ~ 5 hr)	1e-11	–	–	<9e-8	6.7e-11	4e-8

PD-CSD is the same measurement principle used by Give'on *et. al.*¹⁵ and Belikov *et. al.*¹⁶ The latter reported 2.4×10^{-9} in closed loop, which corresponds to 20% of a 1.2×10^{-8} mean speckle contrast, similar to our Milestone 1 performance. But correspondences between open- and closed-loop results must be drawn cautiously. On this study we will extend the previous work by explicitly examining the sensing accuracy separately from other expected effects, such as hysteresis in the DM or a breakdown of the “superposition of influence functions” postulate. One way we might do this is by testing the CSD measurement accuracy at lower mean speckle contrast, or by checking consistency of multiple measurements of speckle-brightness after subtraction of the CSD-derived speckle map. And of course we will repeat these tests with deliberately applied incoherent backgrounds of varying brightness. By these steps, we expect to make progress toward meeting flight requirements for speckle knowledge and control a Jovian- or terrestrial-exoplanet mission.

Wallace *et. al.*²⁰ reported a laboratory demonstration of a reference beam CSD system for a coronagraph on a ground-based telescope, the Gemini Planet Imager (GPI). This work was very successful for that application, but differs in several respects from the concept we plan to use. Our plan is to combine the beams at the science focal plane, to avoid non-common-path systematic errors; and our reference beam is only bright enough to raise the signals above the incoherent signals. Baudoz’s self-coherent camera concept is very similar to this, with Fizeau-type combination.^{21,27}

These experiments with coherent speckle detection are a convincing experimental proof-of-principle (TRL 3). The performance achieved so far (uncertainties of a few times 10^{-10} and passbands <2%) are not quite sufficient for a probe-class mission for direct detection of Jupiter-like

planets. And Biller’s results point to the possibility of significant hurdles in broadening the operating passband to the goal of 20% typically assumed for such missions. The results of the proposed study will demonstrate performance comparable to but in many respects less than required for the mission. Table 1 gives a series of follow-on steps needed to reach TRL 4.

2.3. Differences between flight and laboratory

We will demonstrate the effectiveness of PD-CSD and PH-CSD techniques for post-processing and as a prelude to closed-loop control, and thus advance one or both methods toward TRL 4. These techniques are applicable to both flagship- and probe-class internal coronagraph missions, and offer similar benefits to each. We anticipate that one or both will meet the probe-class performance requirements, and that methods like these will become part of the core assumptions for all internal coronagraph mission concepts.

This study will focus on demonstration of CSD techniques to the accuracy required, but not yet at the low speckle brightness that will be needed for a flight mission. *Rationale:* we want rapid measurements without concerns over long integration times, drift, and detector sensitivity.

In the study we will only use a single passband of >10% width, whereas in flight we hope to use a bandwidth of 20% or more, and repeat the experiment at a series of passbands spanning an octave or more. *Rationale:* This bandwidth is wide enough to show the technique is robust to bandwidth, but not so wide as to become a driving challenge.

We plan to repeat the measurement with a DC background comparable to the average speckle brightness. *Rationale:* Shows the technique’s robustness to such backgrounds.

The earlier EFC experiments^{15,16} demonstrated closed-loop control using the same sensing principles that we call PD-CSD. We plan to try closed-loop control of speckles by this method, and we expect encouraging results; but we stop short of making it a requirement in this milestone, particularly for PH-CSD sensing; that will appear as a milestone in a later study. Instead, we will interleave CSD measurements with PH measurements and compare the speckle knowledge obtained by the two methods. *Rationale:* We must develop the new measurement technique before we know it’s suitable for closed-loop applications.

3. Milestone Procedure

We will conduct experiments on two CSD techniques for speckle measurements, both at the coronagraph testbed at Princeton, and at the HCIT. To prepare for this, we will first develop performance budgets and flow down requirements for both testbed experiments. Then we will install the few additional optics needed for the experiments, and we will install a set of spectral filters with a means of switching easily among them. This prepares the conditions for CSD experiments in each testbed, including images with and without the reference beam.

The first image is measured with the reference field off, and then another with it on. The interference between the prior residual speckle field and the newly created reference field causes comparatively large variations in intensity across the detector. We make another diversity function on the DM, ideally just changing the reference beam’s phase, and take a third image. It is likely we will want a fourth image with a third diversity function, again shifting the phase. We analyze these images together with the known diversity functions to estimate the amplitude and phase of the residual speckles alone as a function of position or spatial frequency. Ideally these images would use a broad optical passband to maximize the information rate, but the images may

have rapid spectral variations, requiring a bandwidth of 1-10%. Demonstration of this technique requires no hardware additions or modification of the existing testbeds.

3.1. Definitions

The contrast metric requires a measurement of the intensity of speckles appearing within the dark field, relative to the intensity of the incident star. The contrast metric will be assessed in terms of statistical confidence to capture the impact of experimental noise and uncertainties. In the following paragraphs we define the terms involved in this process, spell out the measurement steps, and specify the data products.

3.1.1. “Raw” Image and “Calibrated” Image.

Standard techniques for the acquisition of CCD images are used. We define a “raw” image to be the pixel-by-pixel image obtained by reading the charge from each pixel of the CCD, amplifying and sending it to an analog-to-digital converter. We define a “calibrated” image to be a raw image that has had background bias subtracted and the detector responsivity normalized by dividing by a flat-field image. Saturated images are avoided in order to avoid the confusion of CCD blooming and other potential CCD nonlinearities. All raw images are permanently archived and available for later analysis.

3.1.2. Starting from scratch

We define “scratch” to be a DM setting in which actuators are set to a predetermined surface figure that is approximately flat (typically, about 20 volts on each actuator).

3.1.3. Testbed “star” source

We define the “star” to be a small pinhole illuminated with broadband light relayed via optical fiber from a source outside the HCIT vacuum wall (e.g., the super-continuum white light source). The “small” pinhole is to be unresolved by the optical system; e.g., a 5- μm diameter pinhole would be “small” and unresolved by the 40- μm FWHM Airy disk in an f/50 beam at 800 nm wavelength.* This “star” is the only source of light in the optical path of the HCIT. It is a stand-in for the star image that would have been formed by a telescope system.

For both Princeton and HCIT, illumination has a spectral passband of width $\delta\lambda/\lambda_0 > 10\%$, centered at a convenient wavelength λ_0 , such as in the I spectral band, $720 \text{ nm} \leq \lambda_0 \leq 880 \text{ nm}$.

Some tests require a stray light source, which is incoherent with the star. This may be an LED near the detector, or an incandescent lamp outside the chamber, or even a sample of the “star” source carried with several cm of optical path delay.

3.1.4. Contrast map

The “contrast map” is a dimensionless map representing, for each pixel of the detector, the ratio of its intensity value to the value at the peak of the central PSF that would be measured in the same testbed conditions (light source, exposure time, Lyot stop, etc.) if the coronagraph focal plane mask were removed. The calibration of the contrast map is further detailed in Section 3.3.

3.1.5. Speckle field map

The speckle field map is a dimensionless complex-valued map representing the ratio of the optical electric field value at each pixel of the detector to the value at the peak of the central PSF that

* If the beam from the pinhole were substantially overfilling the next few optics, then it would be mostly unresolved by those optics. Normally this ensures the pinhole cannot be distinguished from a perfect point source. But the fact that the pinhole is still partially resolved could have discernible effects in such a sensitive experiment as this. That is a key concern which we hope to resolve my models and experiment during the study.

would be measured in the same testbed conditions (light source, exposure time, Lyot stop, etc.) if the coronagraph focal plane mask were removed. In the absence of stray light, the contrast map is proportional to the absolute value squared of the speckle field map; that is, the speckle field map combines the coherent portion of the contrast map with phase information. The calibration of the speckle field map is further detailed in Section 3.3.

3.1.6. Dark field

The region of the contrast map within which speckles are to be suppressed in preparation for CSD experiments. The dark field chosen for this study is any useful $2 \times 2 \lambda_0/D$ patch within $<10 \lambda_0/D$ of the location of the star.

3.1.7. Contrast value

The “contrast value” is a dimensionless quantity that is the average value of the contrast map over the $2 \times 2 \lambda_0/D$ dark field adopted for the experiment.

3.1.8. Control algorithm

We define the “control algorithm” to be the computer code that takes as input the PD-CSD measurements, and produces as output a voltage value to be applied to each element of the DM, with the goal of reducing the intensity of speckles. During this study we do not plan to develop a corresponding algorithm for CSD-measured speckle fields.

3.1.9. Phase Diversity CSD measurement

We define the “phase diversity coherent speckle detection (PD-CSD) measurement” to be the procedure implementing phase diversity CSD as a method of estimating each speckle’s amplitude and phase, including the changes applied to the DM and the computer code that takes calibrated images and yields estimates of speckle amplitude and phase. Using the results of the PD-CSD measurement to correct the wavefront is optional, as resources allow.

3.1.10. Pinhole CSD measurement

We define the “Pinhole coherent speckle detection (PH-CSD) measurement” to be the procedure implementing PH-CSD (with a separated-path reference beam) as a method of estimating each speckle’s amplitude and phase, including the changes applied to the piston-tip-tilt mirror and the computer code that takes calibrated images and yields estimates of speckle amplitude and phase. Using the results of the PH-CSD measurement to correct the wavefront is optional, as resources allow.

3.1.11. Statistical Confidence

The interpretation of measured numerical contrast values shall take into consideration, in an appropriate way, the statistics of measurement, including detector read noise, photon counting noise, and dark noise.

The milestone objective is to demonstrate with high confidence that the contrast map in the dark field, as estimated from PD-CSD measurements, matches the contrast map as estimated by the PH-CSD measurements, within 20% of the mean contrast value; and that the speckle phase determinations match within 1 radian. The contrast maps shall be obtained from the average of the set of four or more PD measurements in a continuous sequence, interleaved with an equal number of PH measurements.

Every pixel will have two comparable measurements (PD and PH) yielding a contrast map *difference*, in each of several iterations. The first thought is to treat every pixel in every iteration as an independent measurement of the contrast map difference, and to handle the statistics accordingly. This is reflected in the description below. But this isn’t fully realistic: we also expect cor-

relations across each contrast map, particularly within a PSF, which will reduce the number of truly independent samples that can be drawn from each map.

For this milestone the mean contrast value should be $\sim 1 \times 10^{-8}$ in each PD measured contrast map, not as a primary performance criterion, but to establish conditions comparable to flight. Each PH measurement shall be accompanied by an adjacent PD measurement. The primary performance criterion is that the standard deviation of the PD-PH contrast differences shall be less than 20% of the contrast value with a confidence coefficient of 90% or better, and the mean of the PD-PH phase differences shall be less than 1 radian with a confidence coefficient of 90% or better.

Estimation of this statistical confidence level requires an estimation of variances. An analytical development of speckle statistics is impractical, since they include a mix of static speckles (the residual speckle field map remaining after the completion of a wavefront sensing and control cycle) and quasi-static speckles (arising from alignment drift following the control cycle); the superposition of speckles of multiple wavelengths exhibiting their own deterministic wavelength dependencies; and other sources of measurement noise including photon detection statistics and CCD noise. Our approach is to compute the confidence coefficients on the assumption of Gaussian statistics, but also to make the full set of measurements available to enable computation of the confidence levels for other statistics.

The average of one or more images taken at the completion of each iteration is used to compute the contrast map PD_{ij} for iteration i and pixel j . A PH-CSD measurement is made in an adjacent time period, representing the same pattern of speckles, and from that a contrast map PH_{ij} is derived. The mean contrast value for a given iteration i is:

$$C_i = \sum_{j=1}^n \frac{PH_{ij} + PD_{ij}}{2n} \quad (1)$$

where n is the number of independent pixels in the $2 \times 2 \lambda_0/D$ selected dark field of each contrast map. Let us assume that the contrast difference $\Delta_{ij} \equiv PD_{ij} - PH_{ij}$ is a Gaussian-distributed random variable drawn from a parent distribution of zero mean and width σ , where σ includes both technical errors in each measurement and shot noise in the contrast maps. We can calculate the standard deviation in the contrast difference maps for each CSD iteration:

$$\sigma_{\Delta} = \sqrt{\sum_{i=1}^m \sum_{j=1}^n \frac{\Delta_{ij}^2}{mn-1}} \quad \text{where } \Delta_{ij} \equiv PH_{ij} - PD_{ij} \quad (2)$$

Our measured standard deviation σ_{Δ} is an estimate of the parent uncertainty σ . We can calculate the probability density for getting a specific value σ_{Δ} from a set of $m \cdot n$ trials for a certain σ :

$$P(X)dX = \frac{mn}{\Gamma(1+mn/2)\sqrt{2^{mn}}} X^{mn-1} \exp\left(-\frac{1}{2}X^2\right)dX \quad \text{where } X \equiv \frac{\sigma_{\Delta}\sqrt{mn-1}}{\sigma} \quad (3)$$

We can integrate this to find the probability that $\sigma \leq \sigma_0$, where σ_0 is the performance goal, in our case 20% of the mean contrast value. This gives

$$P(\sigma < \sigma_0; \sigma_{\Delta}, mn) = \frac{mn}{\Gamma(1+mn/2)\sqrt{2^{mn}}} \int_{X_0}^{\infty} X^{mn-1} \exp\left(-\frac{1}{2}X^2\right)dX \quad \text{where } X_0 \equiv \frac{\sigma_{\Delta}\sqrt{mn-1}}{\sigma_0} \quad (4)$$

Technology Milestone Whitepaper
Advanced Speckle Sensing for Internal Coronagraphs – Kendrick

This is the statistical confidence level that the measured standard deviations in Equ. 2 meet the goal with sufficient margin. It can be evaluated in closed form for any integer $m \cdot n$. For several values of $m \cdot n$ we can plot the probability vs. σ/σ_0 . This tells us the ratio by which σ_A must be better than the goal (smaller), to know the parent σ is also below the goal with a particular confidence level. These values for $m \cdot n$ are probably much smaller than will be used.

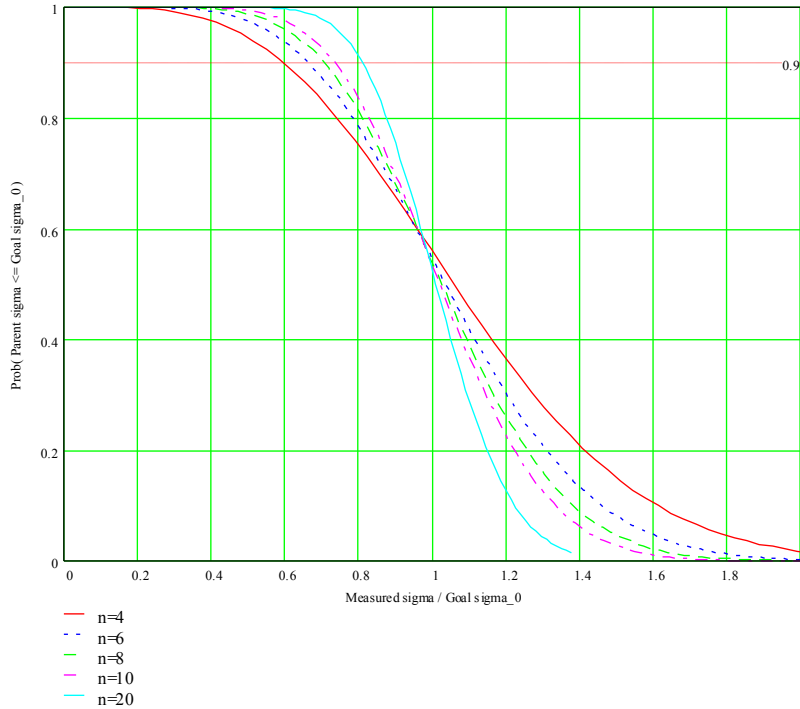


Figure 3 Statistical confidence in the measurement σ ; the probability that the true parent σ is less than the goal σ_0 vs. the measured σ/σ_0 .

3.2. Measurement of the Star Brightness

The brightness of the star is measured with the following steps.

- 3.2.1. The occulting mask is laterally offset, so as to place a transparent region in its transmittance profile at the location of the star image. The transmittance profile of the occulting mask in HCIT is known from imaging data from a microscope CCD camera.
- 3.2.2. To create the photometric reference, a representative sample of short-exposure (e.g. a few milliseconds) images of the star is taken, with all coronagraph elements other than the focal-plane occulting mask in place.
- 3.2.3. The images are averaged to produce a single star image. The “short-exposure peak value” of the star’s intensity is estimated. Since the star image is well-sampled in the CCD focal plane (the Airy disk is sampled by ~ 20 pixels within a radius equal to the FWHM), the star intensity can be estimated using either the value of the maximum-brightness pixel or an interpolated value representative of the apparent peak.
- 3.2.4. The “peak count rate” (counts/sec) is measured for exposure times of microseconds to tens of seconds.

3.3. Measurement of the Coronagraph Contrast map

Each “coronagraph contrast map” is obtained as follows:

- 3.3.1. The occulting mask is centered on the star image.
- 3.3.2. An image (typically exposure times of ~tens of seconds) is taken of the coronagraph field (the suppressed star and surrounding speckle field). Two useful regions, as shown schematically in Fig. 4, are defined as follows: (a) A dark outer (D-shaped) field extending from >3 to $<10 \lambda_0/D$, representing a useful search space, is bounded by a straight line that passes $3-5 \lambda_0/D$ from the star at its closest point, and by a circle of radius $<10 \lambda_0/D$ centered on the star. (b) An inner area within the foregoing dark field, representing contrast in a selected region for all speckle measurement comparisons, is bounded by a square box, each side measuring $2 \times 2 \lambda_0/D$, in a location that captures typical speckles.
- 3.3.3. The image is corrected for the attenuation profile of the occulter and normalized to the “star brightness” as defined in Section 3.2. For this purpose, the fixed relationship between peak star brightness and the integrated light in the speckle field outside the central DM-controlled area will be established, as indicated in Figure 4.²⁸ providing the basis for estimation of star brightness associated with each coronagraph image.

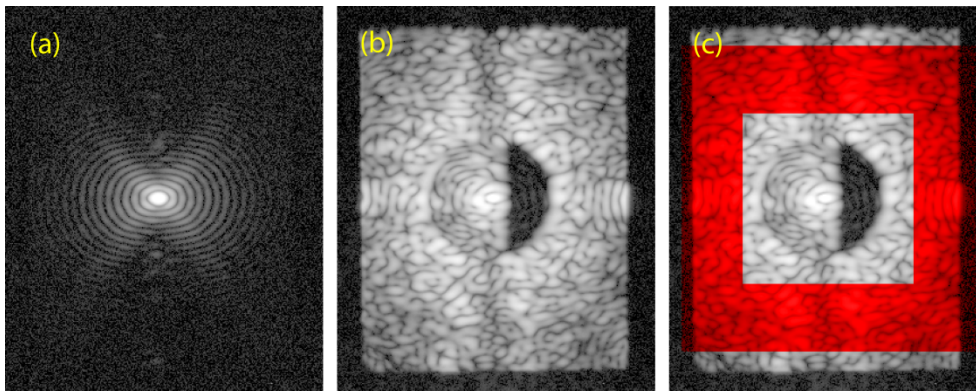


Figure 4 Reference fields for contrast photometry.²⁸ Shown here are (a) the “planet” reference image; (b) the high-contrast coronagraph field; and (c) superimposed in red is the reference speckle field in the “uncontrolled” area beyond the Nyquist limit for the deformable mirror, used as a calibration reference. Images are displayed with a logarithmic contrast grayscale.

- 3.3.4. The contrast map image is averaged over the target high-contrast areas, to produce the contrast value. To be explicit, the contrast value is the sum of all contrast values, computed pixel-by-pixel in the dark field area, divided by the total number of pixels in the dark field area, without any weighting being applied. The rms contrast in a given area can also be calculated from the contrast map image.

3.4. CSD Measurement of the Coronagraph Speckle Field

With the reference field turned off, we measure a focal plane image S_0 . This gives the speckle pattern as it would be during a science observation. Then we activate the reference field and take another image S_1 . We change the reference field, ideally in phase only, and take an image S_2 . Then again change the reference field phase, and take an image S_3 . Let’s say the signals are

$$\begin{aligned}
 S_0 &= c\epsilon_0 E_S^2 + I_Z \\
 S_1 &= c\epsilon_0 \left[E_R^2 + E_S^2 + 2E_R E_S \cos(\phi) \right] + I_Z \\
 S_2 &= c\epsilon_0 \left[E_R^2 + E_S^2 + 2E_R E_S \cos(\phi - \delta) \right] + I_Z \\
 S_3 &= c\epsilon_0 \left[E_R^2 + E_S^2 + 2E_R E_S \cos(\phi + \delta) \right] + I_Z
 \end{aligned} \tag{5}$$

where E_S is the speckle-field amplitude profile across the image, E_R is the reference field profile, ϕ is the phase profile of E_S with respect to E_R , δ is a controlled step in the phase of E_R , and I_Z is the flux of zodi and other incoherent backgrounds.* The images S_0 , S_1 , S_2 , and S_3 can be processed to yield an empirical estimate of E_R via

$$c\epsilon_0 E_R^2 + 2c\epsilon_0 E_R E_S \cos\phi \cdot \cos\delta = \frac{S_2 + S_3}{2} - S_0 \tag{6}$$

Choosing $\delta=\pi/2$ gives an uncomplicated determination of E_R from the images, which is a factor needed for estimates of the speckle field amplitude E_S and phase ϕ of the speckle field:

$$\begin{aligned}
 E_S &= \frac{1}{4c\epsilon_0 E_R} \sqrt{\frac{(S_2 - S_3)^2}{\sin^2 \delta} + \frac{(2S_1 - S_2 - S_3)^2}{(1 - \cos\delta)^2}} \\
 \tan \phi &= \left(\frac{S_2 - S_3}{2S_1 - S_2 - S_3} \right) \tan\left(\frac{\delta}{2}\right)
 \end{aligned} \tag{7}$$

These formulae give roughly uniform emphasis to the three signal measurements in the final results, with no troublesome singularities. Similar analysis is needed if the changes in the reference field E_R are not just an overall phase δ . Also, there may be benefits to using more than 3 different cases for E_R , to overdetermine E_S and ϕ and allow consistency checks.

The determination of ϕ requires an unambiguous reference phase. For this we propose a nearly simultaneous CSD measurement of the phase of the star-leakage field resulting from a deliberate tip-tilt or focus offset of the star from the CFO center.

3.5. Milestone Validation Procedure

A key element of the study is validating the accuracy of the coherent techniques. This is accomplished by applying the statistical tests of Section 3.1.11 to the PH and PD data of Section 3.4. A series of alternating PD and PH measurements are performed, optionally with wavefront correction accompanying each iteration. These are followed by a set of measurements with added stray light. We compute statistics as in Sec. 3.1.11 for PH vs. PD, without incoherent light added; then again with incoherent light added during the measurements. A sufficient number of iterations are performed to allow a statistical measurement with a high enough confidence level.

Other interesting but optional diagnostics are

- comparing CSD results from other wavelength bands, and their co-evolution with time;
- comparing CSD results from the orthogonal polarization, and their co-evolution with time;
- a broadband demonstration of CSD, to show the viability of the technique for a mission.

* The speed of light c and permittivity of free space ϵ_0 are physical constants which calibrate the squared E-fields in $(\text{V}/\text{cm})^2$ to energy fluxes in watt/cm^2 .

They could be performed if resources permit, or saved for a follow-on study.

4. Success Criteria

The following are the required elements of the milestone demonstration. Each element includes a brief rationale.

4.1. Light source

Illumination is spectrally broadband in single or dual polarization, with a bandwidth $\delta\lambda/\lambda_0 > 10\%$, centered at a convenient wavelength λ_0 , such as in the range $720 \text{ nm} \leq \lambda_0 \leq 880 \text{ nm}$.

Rationale: Wavelengths in this range are representative of the science band used by future missions. The bandwidth, although less than would be used in a flight mission, provides an appropriate challenge for this milestone.

4.2. Contrast performance

As a starting point for measurements, a mean contrast value less than 1×10^{-8} should be achieved in a $2 \times 2 \lambda_0/D$ region centered at any convenient location $< 10 \lambda_0/D$ from the star position.

The contrast maps as measured by PH and PD measurement shall match with a standard deviation of 20% of the contrast value, with 90% confidence. The speckle field phase measurements by these two methods shall match with a standard deviation of 1 radian, with 90% confidence.

In the series of interleaved wavefront measurements and DM corrections using PH and PD, described in Section 3.5 above, each cycle will be preceded and followed by equivalent time series of open-loop measurements taken at the same baseline contrast. These additional measurements will allow the open-loop stability of speckles in the testbed to be characterized.

These success criteria shall be quantified in terms of the standard deviation of differences and statistical confidence defined in Eqs. 2 and 4 of Section 3.1.11.

Rationale: The mean contrast is low enough to be in the same optical regime as normal science observations. The uncertainty is comparable to the desired fractional uncertainty for calibration and subtraction of the speckle pattern to reveal a planet. Phase accuracy below 1 radian helps speed closed-loop convergence.

4.3. Incoherent stray light background

The tests described in Section 4.2 will be repeated with added uniform incoherent stray light brighter than the mean speckle contrast (nominally 1×10^{-8} of the star's peak). The contrast maps measured by CSD in the presence of added stray light (but excluding that DC offset) must match those measured by CSD without added stray light, with a standard deviation of 20% of the contrast value, with 90% confidence. The speckle field phase measurements likewise must match with a standard deviation of 1 radian, with 90% confidence.

Rationale: This demonstrates the milestone performance with stray light, one of the key measurement challenges.

4.4. Duration and robustness

Criteria 4.2 and 4.3, averaged over the data set, shall be met with a confidence of 90% or better, as defined in Section 3.1.11. Sufficient data must be taken to justify this statistical confidence.

Rationale: Until we attempt to close the wavefront control loop using CSD measurements, the rms difference of contrast measurements obtained from this dataset provides our best estimate of the contrast measurement uncertainties. Assuming the contrast differences have a Gaussian distribution about zero, this demonstrates a statistical confidence of 90% that the CSD contrast measurement goal has been reached.

Criteria 4.2 and 4.3 must be satisfied on three separate occasions with a reset of the wavefront control system software (DM set to scratch) between each demonstration.

Rationale: This provides evidence of the repeatability of the contrast measurement demonstration. The wavefront control system software reset and re-optimization between data sets ensures that the three data sets can be considered as independent and do not represent an unusually good configuration that cannot be reproduced. For each demonstration the DM will begin from a "scratch" setting and the algorithm used to converge will have no memory of settings used for prior demonstrations, so that we can expect the speckles to be measured are quite different each time. There is no time requirement for the demonstrations, other than the time required to meet the statistics stipulated in the success criteria. There is no required interval between demonstrations; subsequent demonstrations can begin as soon as prior demonstrations have ended. There is also no requirement to turn off power, open the vacuum tank, or delete data relevant for the calibration of the DM influence function.

5. Certification Process

The Principal Investigator will assemble a milestone certification data package for review by the Exoplanet Exploration Program (ExEP) and its Technology Advisory Committee (ExEP-TAC). In the event of a consensus determination that the success criteria have been met, the ExEP will submit the findings of the ExEP-TAC, together with the certification data package, to NASA HQ for official certification of milestone compliance. In the event of a disagreement between the ExEP and the ExEP-TAC, NASA HQ will determine whether to accept the data package and certify compliance or request additional work.

5.1. Milestone Certification Data Package

The milestone certification data package will contain the following explanations, charts, and data products, with estimates of accuracy where appropriate.

1. A narrative report, including a discussion of how each element of the milestone was met, an explanation of each image or group of images, appropriate tables and summary charts, and a narrative summary of the overall milestone achievement.
2. A description of the optical elements, their significant characteristics, and their layout in the HCIT.
3. A tabulation of the significant operating parameters of the apparatus, including temperature stability.
4. A calibrated image of the reference star, and an estimate of photometry errors.

Technology Milestone Whitepaper
Advanced Speckle Sensing for Internal Coronagraphs – Kendrick

5. Calibrated images of the occulter transmittance pattern and/or the measured transmittance profile.
6. Spectrum of the broadband light and an estimate of the intensity uniformity and stability of the illumination reaching the defining pupil (at the DM).
7. A contrast map image representative, within error limits, of the super set of data, with appropriate numerical or color-coded or grey-scale coded contrast values indicated, and with coordinate scales indicated in units of Airy distance (λ_0/D); and the corresponding contrast map for the CSD determination in an adjacent time period.
8. A phase map image representative, within error limits, of the super set of data, with appropriate numerical or color-coded or grey-scale coded contrast values indicated, and with coordinate scales indicated in units of Airy distance (λ_0/D); and the corresponding phase map for the CSD determination in an adjacent time period.
9. The PH-PD phase difference standard deviation for the $2 \times 2 \lambda_0/D$ target area for each data set comprising several consecutive iterations, and for all relevant data sets, in tabular form.
10. The PH-PD contrast difference standard deviation with vs. without stray light, for the $2 \times 2 \lambda_0/D$ target area for each data set comprising several consecutive iterations, and for all relevant data sets, in tabular form.

6. References

- ¹ M. Levine, S. Shaklan, and J. Kasting, "Terrestrial Planet Finder Coronagraph Science and Technology Definition Team (STDT) Report," NASA Jet Propulsion Laboratory, JPL Document D-34923, (2006), http://planetquest.jpl.nasa.gov/TPF/STDT_Report_Final_Ex2FF86A.pdf
- ² J.T. Trauger *et. al.*, "The Eclipse mission: a direct imaging survey of nearby planetary systems," in Proc. SPIE **4854**, *Future EUV/UV and Visible Space Astrophysics Missions and Instrumentation*, J.C. Blades and O. Siegmund, eds. (SPIE, Waikoloa, HI, USA, 2003), pp. 116-128.
- ³ M. Clampin *et. al.*, "Extrasolar Planetary Imaging Coronagraph (EPIC)," in Proc. SPIE **6265**, *Space Telescopes and Instrumentation I: Optical, Infrared, and Millimeter*, J. C. Mather, H.A. MacEwen, and M.W.M. de Graauw, eds. (SPIE, Orlando, FL, USA, 2006), p. 62651B.
- ⁴ O. Guyon *et. al.*, "Pupil mapping Exoplanet Coronagraphic Observer (PECO)," in Proc. SPIE **7010**, *Space Telescopes and Instrumentation 2008: Optical, Infrared, and Millimeter*, J.M. Oschmann Jr., M.W.M. de Graauw, and H.A. MacEwen, eds. (SPIE, Marseille, France, 2008), p. 70101Y.
- ⁵ Technology Readiness Level definitions, NASA Procedural Requirements 7120.8 Appendix J, http://nodis3.gsfc.nasa.gov/displayDir.cfm?Internal_ID=N_PR_7120_0008_&page_name=AppendixJ
- ⁶ G. Schneider, R. I. Thompson, B. A. Smith and R. J. Terile, "Exploration of the environments of nearby stars with the NICMOS coronagraph: instrumental performance considerations," in Proc. SPIE **3356**: *Space Telescopes and Instruments V*, P.Y. Bely and J.B. Breckinridge, Eds., pp. 222-233, SPIE, Kona, HI, USA (1998).
- ⁷ W. Sparks, R. Brown, C. Burrows, M. Clampin, J. E. Krist, H. Ford, P. D. Feldman, and D. Golimowski, "Detection of Planets with the Hubble Space Telescope Advanced Camera," in *Bioastronomy 99* (Kohala Coast, HI, 1999), G. Lemarchand, and K. Meech, eds., ASP Conference Series **213**, p. 131.
- ⁸ S. R. Heap, D. J. Lindler, T. M. Lanz, R. H. Cornett, I. Hubeny, S. P. Maran and B. E. Woodgate, "Space Telescope Imaging Spectrograph Coronagraphic Observations of beta Pictoris," *Astrophys. J.* **539**(1), 435 (2000)

Technology Milestone Whitepaper

Advanced Speckle Sensing for Internal Coronagraphs – Kendrick

- ⁹ V. G. Ford et. al., “Terrestrial Planet Finder Coronagraph Flight Baseline 1 Design Report,” NASA Jet Propulsion Laboratory, presented at the TPF-C STDT Meeting, New York, NY (Sept 2005), <http://hdl.handle.net/2014/38071>
- ¹⁰ R. Racine, G. A. H. Walker, D. Nadeau, R. Doyon and C. Marois, “Speckle Noise and the Detection of Faint Companions,” *PASP* 111(759), 587-594 (1999)
- ¹¹ C. Marois, R. Doyon, R. Racine and D. Nadeau, “Efficient Speckle Noise Attenuation in Faint Companion Imaging,” *PASP* 112(767), 91-96 (2000)
- ¹² C. Marois, R. Doyon, R. Racine and D. Nadeau, “Differential imaging coronagraph for the detection of faint companions,” in Proc. SPIE 4009: *Optical and IR Telescope Instrumentation and Detectors*, M. Iye and A. F. M. Moorwood, Eds., pp. 788-796, SPIE, Munich, Germany (2000).
- ¹³ J. T. Trauger, C. J. Burrows, B. Gordon, J. J. Green, A. E. Lowman, D. Moody, A. F. Niessner, F. Shi and D. Wilson, “Coronagraph contrast demonstrations with the high-contrast imaging testbed,” in Proc. SPIE **5487: Optical, Infrared, and Millimeter Space Telescopes**, J. C. Mather, ed., pp. 1330-1336, Glasgow, Scotland, UK (2004).
- ¹⁴ P. Bordé and W. Traub, “High-Contrast Imaging from Space: Speckle Nulling in a Low-Aberration Regime,” *Astrophysical Journal* **638**, 488-498 (2006).
- ¹⁵ A. Give'on, R. Belikov, S. Shaklan, and J. Kasdin, “Closed loop, DM diversity-based, wavefront correction algorithm for high-contrast imaging systems,” *Optics Express* **15**, 12338-12343 (2007).
- ¹⁶ R. Belikov, A. Give'on, B. Kern, E. Cady, M. Carr, S. Shaklan, K. Balasubramanian, V. White, P. Echternach, M. Dickie, J. Trauger, A. Kuhnert and N. J. Kasdin, “Demonstration of high contrast in 10% broadband light with the shaped pupil coronagraph,” in Proc SPIE **6693: Techniques and Instrumentation for Detection of Exoplanets III**, D.R. Coulter, ed., p. 66930Y, San Diego, CA (2007).
- ¹⁷ R. Belikov, A. Give'on, D. Savransky, L. Pueyo, B. Kern, and J. Kasdin, “Demonstration Of Synthetic Exo-earth Detection In The Lab With Speckle Subtraction Techniques,” in AAS **211**, Bulletin of the American Astronomical Society, (2008), p. 975.
- ¹⁸ O. Guyon, “Imaging Faint Sources within a Speckle Halo with Synchronous Interferometric Speckle Subtraction,” *Astrophysical Journal* **615**, 562-572 (2004).
- ¹⁹ J. L. Codona, and R. Angel, “Imaging Extrasolar Planets by Stellar Halo Suppression in Separately Corrected Color Bands,” *Astrophysical Journal Letters* **604**, L117-L120 (2004).
- ²⁰ J.K. Wallace, J. Angione, R. Bartos, P. Best, R. Burruss, F. Fregoso, B.M. Levine, B. Nemati, M. Shao and C. Shelton, “Post-coronagraph wavefront sensor for Gemini Planet Imager,” in Proc SPIE **7015: Adaptive Optics Systems**, N. Hubin, C.E. Max and P.L. Wizinowich, eds., p. 70156N, Marseille, France (2008).
- ²¹ P. Baudoz, A. Boccaletti, J. Baudrand and D. Rouan, “The Self-Coherent Camera: a new tool for planet detection,” in Proc. *IAU 200: Direct Imaging of Exoplanets: Science & Techniques* C. Aime and F. Vakili, Eds., pp. 553-558, Cambridge University Press, Nice, France (2005).
- ²² J. T. Trauger, and W. A. Traub, "A laboratory demonstration of the capability to image an Earth-like extrasolar planet," *Nature* **446**, 771-773 (2007)
- ²³ R. Belikov, N. J. Kasdin, R. Vanderbei, and M. Carr, “Demonstration of Gains in Exoplanet Imaging Sensitivity in a Shaped Pupil Coronagraph by Use of the Differential Image Technique,” in AAS **#207**, Bulletin of the American Astronomical Society, (2005), p. 1412.
- ²⁴ B. Biller, J. Trauger, D. Moody, L. Close, A. Kuhnert, K. Stapelfeldt, W. A. Traub, and B. Kern, “A Multi-wavelength Differential Imaging Experiment for the High Contrast Imaging Testbed,” *PASP* **121**, 716-727 (2009).
- ²⁵ R. Belikov, A. Give'on, E. Cady, J. Kay, L. Pueyo, and N. J. Kasdin, “Experimental Demonstration of Wavefront Estimation in a Shaped-Pupil Coronagraph,” in AAS **#209**, Bulletin of the American Astronomical Society, (2007), p. 1131. <http://www.docsntalks.com/go/XPL573>

Technology Milestone Whitepaper
Advanced Speckle Sensing for Internal Coronagraphs – Kendrick

²⁶ Guyon et. al., in preparation

²⁷ R. Galicher, P. Baudoz, G. Rousset, J. Totems and M. Mas, “Self-coherent camera as a focal plane wavefront sensor: simulations,” *A&A* 509(A31) (2010)

²⁸ J. T. Trauger, B. Kern, and A. Kuhnert, “TPF-C Milestone #1 Report,” JPL Document D-35484, July 2006.

Appendix A. Uncertainty and integration time analysis

For both methods, we create a reference field E_R , which interferes coherently with the speckle field E_S , producing a heterodyne signal that rises above the zodi shot noise or other background noise sources. This allows quicker measurements, one of the principal benefits of CSD. The strength of the reference field has a practical limitation from the need to control measurement uncertainty caused by the reference beam's own imperfections.

After the coronagraph instrument has completed an initializing coarse wavefront control procedure, E_S is small enough that its intensity $c\epsilon_0|E_S|^2$ at the science detector* is comparable to the zodi signals in each pixel. At that point, it becomes much more time-consuming to continue measuring a progressively smaller $c\epsilon_0|E_S|^2$ by itself. When we introduce E_R , either by adding a diversity function to the DM settings or by enabling the pickoff beam from the CFO, the intensity of the combined fields at the detector array is

$$c\epsilon_0|E_R + E_S|^2 = c\epsilon_0\left[|E_R|^2 + |E_S|^2 + 2|E_R E_S|\cos(\phi_0)\right] \quad (\text{A.1})$$

where ϕ is the relative phase of E_R and E_S . If we choose a large enough E_R , we can make the interference term, $2c\epsilon_0|E_R E_S|\cos(\phi)$, larger than the background signals, speeding the measurement. (If $E_R > E_S$, the heterodyne term $2E_R E_S$ is larger than the speckle term E_S^2 ; this is known as ‘‘heterodyne amplification.’’) And by exercising ϕ via the phase of E_R , we can also measure the phase of E_S . Knowing both the amplitude and phase of E_S allows us to adjust the DM correctly on the first try, to cancel E_S .

The shot-noise-limited signal to noise ratio (SNR) on the measurement of the amplitude of the heterodyne term is

$$SNR_h = \frac{2c\epsilon_0 E_R E_S T}{\sqrt{2(c\epsilon_0 E_R^2 + c\epsilon_0 E_S^2 + I_z)T}} \quad (\text{A.2})$$

where I_z is the background flux from local and exo-zodiacal light, and T is the integration time. But SNR_h represents $E_R E_S / \sigma(E_R E_S)$, whereas we want $E_S^2 / \sigma(E_S^2)$. That is, we plan to calibrate E_S with E_R turned on, and from that estimate and subtract the speckle intensity $c\epsilon_0 E_S^2$. So what we really care about is the uncertainty in the speckle alone:

$$\frac{1}{SNR_S} = \frac{2E_S \sigma_{E_S}}{E_S^2} = 2 \frac{\sigma_{E_S}}{E_S} \quad (\text{A.3})$$

whereas the uncertainty in the heterodyne measurement has a different dependence:

$$\frac{1}{SNR_h} = \frac{\sigma(2E_R E_S)}{2E_R E_S} = \sqrt{\frac{\sigma_{E_R}^2}{E_R^2} + \frac{\sigma_{E_S}^2}{E_S^2}} \quad (\text{A.4})$$

So the uncertainty in the speckle alone is

$$\frac{1}{SNR_S} = 2 \frac{\sigma_{E_S}}{E_S} = 2 \sqrt{\frac{1}{SNR_h^2} + \frac{\sigma_{E_R}^2}{E_R^2}} = 2 \sqrt{\frac{2(c\epsilon_0 E_R^2 + c\epsilon_0 E_S^2 + I_z)}{(2c\epsilon_0 E_R E_S)^2 T} + \frac{\sigma_{E_R}^2}{E_R^2}} \quad (\text{A.5})$$

* The speed of light c and permittivity of free space ϵ_0 are physical constants which calibrate the squared E-fields in $(\text{V}/\text{cm})^2$ to energy fluxes in watt/cm^2 .

Technology Milestone Whitepaper
Advanced Speckle Sensing for Internal Coronagraphs – Kendrick

The procedure for estimating these quantities from measurements comprises taking at least 3 and probably 4-7 signal measurements: one without E_R and 2-6 with E_R at different optical phases. (Redundancy of the measurements affords a degree of robustness as well as a chance to detect systematic variability.) That analysis gives a metric for estimating E_s based on those signals. That in turn gives an estimator of the uncertainty in E_s via that metric.

We have preliminary estimates of the shot noise limited integration time for calibrating a speckle to SNR=10. Figure 5 shows the integration time as a function of the normalized reference beam brightness R_{Rz} , for a Lyot coronagraph of 1.5m diameter, a $V=6$ star, and a fixed speckle brightness which is 10^{-9} of the star. For a speckle nulling detection of the speckle brightness (reference brightness = speckle brightness), the integration time for 10% uncertainty is 5.8 hr. Measuring the speckle field via CSD, we need an uncertainty $<5\%$

to estimate the speckle brightness to 10%; this can be accomplished in as little as 10 min. This analysis helps us choose the reference beam amplitude. Note that Figure 5 includes an improvement in σ_{E_R}/E_R with increasing E_R , due to improving shot noise in the measurement of the reference beam brightness.

We can also estimate the time needed to calibrate the speckles as a function of the zodi flux. We know very little about the typical exozodi contribution for the favored exoplanet target stars, so an important figure of merit for each mission concept is its robustness to elevated exozodi levels (above our local zodi). As shown in Figure 6, the CSD methods have essentially constant integration time with increasing exozodi level, while a direct speckle measurement scales linearly with zodi flux. In this analysis the reference beam flux is always 3 times the zodi flux; but at some exozodi level, this scaling may have to be abandoned due to systematic errors, and thereafter the curve will turn upward.

Thus for high-zodi stars, planet detection would still take a correspondingly longer integration time, but the speckle calibration could be almost as brief as for lower-zodi stars. This allows us to continue using a quick-cycle timeline with calibrations taking a few hours or less, and simply extend the total observing time on that target. But for direct speckle detection, calibration itself quickly becomes an infeasibly lengthy process, and instrument drift becomes much more uncertain. This is a key driver for the minimum planet sensitivity.

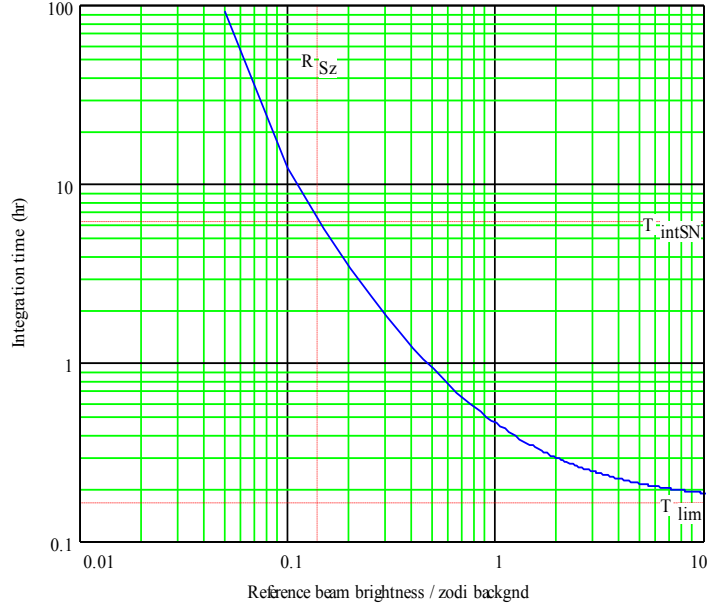


Figure 5 Integration time (sec) for speckle calibration as a function of reference beam intensity, for a 1.5m diameter Lyot coronagraph. R_{Rz} is the reference beam brightness scaled to the zodi+exozodi background; R_{Sz} is the speckle brightness scaled likewise, and we find $R_{Sz} \approx 1/7$; T_{intSN} is the integration time for a speckle-nulling measurement of speckle brightness to SNR=10, *i.e.* with $R_{Rz} = R_{Sz}$ (5.8 hr). Solid red line shows the integration time for estimating the same quantity using CSD. T_{lim} is the asymptotic integration time, equal to the shot-noise-limited integration time for the speckle with no background signals.

Technology Milestone Whitepaper
Advanced Speckle Sensing for Internal Coronagraphs – Kendrick

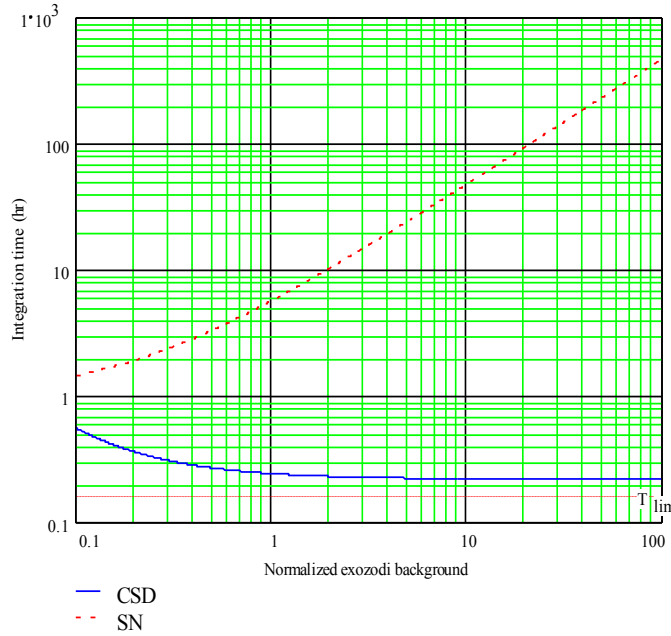


Figure 6 Integration time (hr) vs. zodi flux for CSD and SN measurements. CSD (solid red line) uses a reference beam that is 3 times the zodi flux; SN (dashed blue line) uses a reference beam just as bright as the speckle. The CSD integration time is nearly independent of zodi flux as long as this scaling is feasible. But speckle calibration by direct measurement may not remain practical on high-zodi stars.

Technology Milestone Whitepaper
Advanced Speckle Sensing for Internal Coronagraphs – Kendrick